C. R. Chimie 18 (2015) 644–653

Contents lists available at ScienceDirect

Comptes Rendus Chimie

www.sciencedirect.com

Full paper/Mémoire

Effect of pretreatment gases on the performance of WO_3/SiO_2 catalysts in the metathesis of 1-butene and ethene to propene

Huan Liu [a,b], Kai Tao [a], Hongbo Yu [a], Chen Zhou [a], Zhen Ma [c,*], Dongsen Mao [b,*], Shenghu Zhou [a,*]

[a] Ningbo Institute of Materials Technology and Engineering, Chinese Academy of Sciences, 1219, Zhongguan West Road, Ningbo, Zhejiang 315201, China
[b] Research Institute of Applied Catalysis, Shanghai Institute of Technology, 100, Haiquan Road, Shanghai 201418, China
[c] Department of Environmental Science and Engineering, Fudan University, Shanghai 200433, China

ARTICLE INFO

Article history:
Received 10 June 2014
Accepted after revision 17 November 2014
Available online 16 May 2015

Keywords:
Propene
Metathesis
Disproportion
WO_3/SiO_2 catalysts
Gas pretreatment

ABSTRACT

Different gases were employed to pretreat WO_3/SiO_2 for the metathesis of 1-butene and ethene to propene. Air-pretreated WO_3/SiO_2 was inactive, whereas N_2-, N_2/H_2-, and H_2-pretreated WO_3/SiO_2 exhibited high 1-butene conversion and propene selectivity. Tetragonal WO_3 and partially reduced $WO_{2.92}$ were found to be the active phases/species, whereas monoclinic WO_3 was inactive. N_2/H_2- and H_2-pretreated WO_3/SiO_2 contained both W^{6+} and W^{5+} species (i.e., nonstoichiometric WO_{3-x}). Air- and N_2-pretreated WO_3/SiO_2 only contained monoclinic W^{6+} species (WO_3) before the reaction. However, the used N_2-pretreated WO_3/SiO_2 contained both W^{6+} and W^{5+} species, suggesting that the N_2 pretreatment can facilitate the formation of some W^{5+} species during the reaction. This in situ partial reduction can activate the N_2-pretreated WO_3/SiO_2 for the metathesis.

1. Introduction

Olefin metathesis, first reported by Banks and Bailey in 1964 [1], is an important method for the production of fine chemicals and polymers [2–4]. Supported W [5–9], Mo [10–12], and Re [13,14] catalysts have been intensively studied for olefin metathesis. Among them, Re_2O_7/Al_2O_3 exhibits higher activity and selectivity at low reaction temperatures [15,16], but the high price of Re limits its wide applications. Although WO_3/SiO_2 is less active than Re_2O_7/Al_2O_3 and MoO_3/Al_2O_3, it is the most widely used in industry for the metathesis of butene and ethene due to its excellent stability and resistance to poisoning [17,18]. In a typical process, 2-butene and ethene react to produce propene, and 1-butene in the butene mixture has to first isomerize to 2-butene in order to form propene [19]. Generally, a conversion of 65–70% and a propene selectivity of 90% were obtained on WO_3/SiO_2 at 250–300 °C, as reported by ABB Lummus [6]. MgO [19] was used together with WO_3/SiO_2 to isomerize 1-butene in the butene mixture to 2-butene in industrial processes.

The pretreatment conditions of supported WO_3 catalysts were found to influence the oxidation state of W, thus affecting its catalytic performance [20–24]. Choung and Weller pretreated WO_3/SiO_2 with N_2 or H_2 to form some WO_{3-x} intermediates regarded as catalytically active species [25]. Westhoff and Moulijn found that slightly reduced WO_3/SiO_2 catalysts showed higher activity in metathesis than calcined samples, and a tungsten oxide composition between WO_3 and $WO_{2.95}$ (formed by H_2 reduction of WO_3/SiO_2 at 875 K) exhibited the highest

* Corresponding authors.
E-mail addresses: zhenma@fudan.edu.cn (Z. Ma), dsmao@sit.edu.cn (D. Mao), zhoush@nimte.ac.cn (S. Zhou).

http://dx.doi.org/10.1016/j.crci.2014.11.008
1631-0748/

activity [26]. Basrur et al. inferred the formation of $WO_{2.9}$ through the appearance of a blue-violet color of the used catalyst, and $WO_{2.9}$ was regarded as the active species in metathesis [27]. Huang et al. reported that the activity of 10 W/Al_2O_3–*x* HY increased with the increase in the zeolite content (HY) [28]. When the zeolite content exceeded 70%, the activity decreased due to the deep reduction in W^{6+} species. Zaki et al. reported that WO_3 could form three intermediate nonstoichiometric oxidation states ($WO_{2.96}$, $WO_{2.9}$, and $WO_{2.72}$) by H_2 reduction and the formation process could be adjusted by controlling the reduction conditions [29,30].

Although attempts have been made to explore the active species of WO_3/SiO_2 catalysts for the metathesis of 1-butene and ethene, there was no systematical investigation of the active species through comprehensive characterization and no systematical research about the effect of pretreatment gases on the catalytic performance. Herein, a systematical research about the change in the physicochemical properties of WO_3/SiO_2 pretreated by air, N_2, N_2/H_2, and H_2 was conducted by comprehensive characterization, and the catalytically active tungsten oxide phase/species were assigned. The correlation between the active tungsten oxide phase/species and the catalytic performance for the metathesis of 1-butene and ethene was concluded.

2. Experimental

2.1. Catalyst preparation

The SiO_2 support (surface area 399.1 m^2/g, size 3–5 mm) was obtained from Qingdao Haiyang Chemical Co. Ltd., and ammonium metatungstate (AR) was purchased from Sinopharm Chemical Reagent Co. Ltd. MgO tablets (surface area 78.13 m^2/g, size 4–5 mm) were prepared by direct compression of MgO powders (99.99%) purchased from Aldrich. WO_3/SiO_2 (6.0 wt% WO_3) was prepared by incipient-wetness impregnation of SiO_2 by an aqueous solution of ammonium metatungstate followed by drying at 120 °C for 12 h and calcination in the air at 460 °C for 4 h. The obtained catalyst, denoted as WS, will be further treated by different gases in a fixed-bed catalytic reactor.

2.2. Catalyst pretreatment process and catalytic testing

Nineteen grams of WS (WO_3/SiO_2 without any gas pretreatment) were blended with 76.0 g MgO tablets, and then loaded into a fixed-bed reactor (internal diameter 3.3 cm). The catalyst was first heated to 400 °C in N_2 with a flow rate of 1.0 L/min. At 400 °C, N_2, 1/9 H_2/N_2 (v/v), 1/1 H_2/N_2 (v/v), or H_2 (flow rate 1.0 L/min) were fed into the reactor to treat the catalyst for 30 min. The reactor was further heated to 550 °C and maintained at 550 °C for 2 h under N_2 (flow rate 1.0 L/min). The reactor was then cooled down to 280 °C under N_2 (flow rate 1.0 L/min), followed by feeding 1-butene and ethene at 280 °C and 3.0 MPa, and at a weight hourly space velocity (WHSV, 1-butene + ethene) of 1.49 h^{-1} with a 1.6/1.0 molar ratio of ethene/1-butene. The flow rate of ethene was monitored by a mass-flow controller, and 1-butene was pumped into the system and gasified in a preheater. The above catalysts pretreated by N_2, 1/9 H_2/N_2 (v/v), 1/1 H_2/N_2 (v/v), or H_2 were denoted as WS–N_2, WS–1/9H_2/N_2, WS–1/1H_2/N_2, or WS–H_2, respectively.

To obtain air-pretreated WO_3/SiO_2 (WS–air), WS blended with MgO was first heated to 400 °C in the air (flow rate 1.0 L/min). At 400 °C, air (flow rate 1.0 L/min) was fed into the reactor to treat the catalyst for 30 min. The reactor was further heated to 550 °C and maintained at 550 °C for 2 h under air (flow rate 1.0 L/min) to get rid of residual water. The reactor was then cooled down to 280 °C under air (flow rate 1.0 L/min), which was followed by feeding the reactants. The reaction conditions for WS–air were the same as those described above.

The reaction products were analyzed online using a gas chromatograph equipped with a flame ionization detector (FID), and 1-butene conversion and propene selectivity were calculated according to the literature [28,31].

2.3. Catalyst characterization

Inductively coupled plasma (ICP) analysis was performed on a PerkinElmer OPTIMA 2100 DV optical emission spectroscopy spectrometer to identify the real tungsten oxide contents in the WO_3/SiO_2 catalysts. Brunauer–Emmett–Teller (BET) surface areas, pore volumes, and pore sizes were obtained using a Micromeritics ASAP 2020 M adsorption apparatus. Prior to measurement, the sample was degassed under vacuum at 200 °C for 3 h. X-ray diffraction (XRD) patterns were recorded with a D8 Advance X-Ray Diffractometer using Cu Kα radiation in the 2θ range from 10° to 70°. Raman spectra were obtained using a Renishaw Raman Spectrometer equipped with a microscope (laser wavelength: 532 nm). UV–vis spectra were recorded using a PE Lambda950 with $BaSO_4$ as a reference.

The images of transmission electron microscopy (TEM) and high-resolution transmission electron microscopy (HRTEM) were recorded on a Tecnai F20 Transmission Electron Microscope. The samples were prepared as follows: the catalysts were dispersed in ethanol by sonication, and a few drops of the dispersion were dropped onto a carbon-coated copper grid, which was followed by solvent evaporation in the air at room temperature.

X-ray photoelectron spectroscopy (XPS) data were recorded by a Kratos AXIS ULTRA DLD X-ray photoelectron spectrometer using Al Kα as the exciting source. Data processing was performed using CasaXPS software. The spectra were fit after linear background subtraction.

H_2 temperature-programmed reduction (H_2-TPR) was carried out in a quartz microreactor. The as-prepared samples (50 mg) were pretreated at 300 °C in Ar for 1 h prior to H_2-TPR measurement, which was followed by a temperature-programmed reduction by 1/10 H_2/Ar flow (v/v, 50 mL/min) from room temperature to 800 °C with a ramping rate of 5 °C/min. Hydrogen consumption was monitored by a thermal conductivity detector (TCD).

The infrared (IR) spectra of the samples were obtained in a transmission mode in a Bruker Tensor 27 spectrophotometer. A Pyris Diamond thermogravimetric analyzer

Table 1
Specific surface areas, pore volumes, and mean pore sizes of WO_3/SiO_2 catalysts pretreated by different gases.

Catalysts	BET surface area (m^2/g)	Pore volume (cm^3/g)	Average pore size (nm)
WS–air	332	0.83	7.5
WS–N_2	345	0.83	7.2
WS–1/9H_2/N_2	344	0.84	7.3
WS–1/1H_2/N_2	339	0.89	8.3
WS–H_2	349	0.88	7.8

(TGA) was used to analyze the organic residues in the used catalysts. The experimental run was carried out from 50 to 800 °C with a heating rate of 10 °C/min in flowing air (flow rate 50 mL/min).

3. Results and discussion

The BET surface areas, pore volumes, and mean pore sizes of WO_3/SiO_2 catalysts with an actual WO_3 content of 6.0 wt% determined by ICP are summarized in Table 1. All catalysts after different gas pretreatments showed insignificant changes of BET surface areas, and a slight change in pore volume and pore size was found in 1/1H_2/N_2 and H_2-pretreated catalysts.

XRD patterns of WO_3/SiO_2 catalysts are shown in Fig. 1. As shown in Fig. 1b and 1c, WS-air and WS–N_2 exhibited similar XRD patterns assigned to monoclinic WO_3. In contrast, WS–1/9H_2/N_2 (Fig. 1d) and WS–1/1H_2/N_2 (Fig. 1e) exhibited XRD patterns assigned to tetragonal WO_3, suggesting that the thermal treatment of WS in the presence of H_2/N_2 mixtures induced the phase change of WO_3. When pure H_2 was used to pretreat WS, nonstoichiometric $WO_{2.92}$ phase appeared (Fig. 1f), indicating the partial reduction of WO_3 [29].

XPS data of WO_3/SiO_2 after different gas pretreatments are shown in Fig. 2. The XPS curve fitting procedure is that of Doniach and Sunjic [32]. The binding energies of

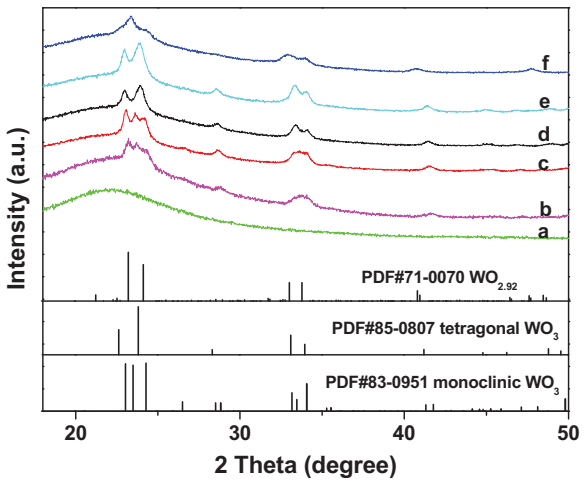

Fig. 1. (Color online.) XRD patterns of 6.0 wt% WO_3/SiO_2 catalysts pretreated with different gases: (a) commercial SiO_2, (b) WS–air; (c) WS–N_2; (d) WS–1/9H_2/N_2; (e) WS–1/1H_2/N_2; (f) WS–H_2.

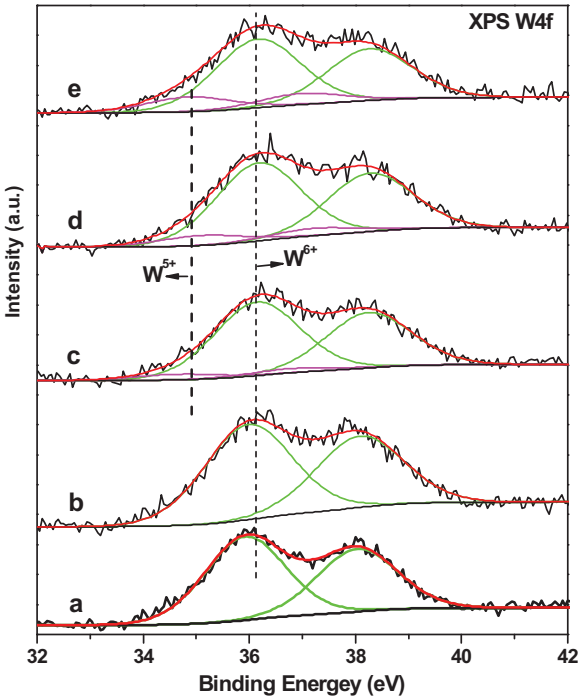

Fig. 2. (Color online.) XPS spectra of 6.0 wt% WO_3/SiO_2 catalysts pretreated with different gases: (a) WS–air; (b) WS–N_2; (c) WS–1/9H_2/N_2; (d) WS–1/1H_2/N_2; (e) WS–H_2.

35.9 and 38.0 eV in Fig. 2a for WS–air were assigned to $4f_{7/2}$ and $4f_{5/2}$ of W^{6+} (WO_3), respectively [33–35]. As shown in Fig. 2b, WS–N_2 exhibited the similar XPS data as WS–air; only W^{6+} was observed. For WS–1/9H_2/N_2, WS–1/1H_2/N_2, and WS–H_2, in addition to the binding energies of W^{6+}, the binding energies of 34.6∼35.1 eV and 36.7∼37.2 eV can be assigned to $4f_{7/2}$ and $4f_{5/2}$ of W^{5+} [36–39], respectively, confirming the partial reduction of a small portion of WO_3 by H_2 or H_2/N_2 pretreatment. The intensities of XPS peaks of W^{5+} increased with the increase in the H_2 content in the gases.

Table 2 summarizes the molar percentages of W^{6+} and W^{5+} obtained by XPS for different gas-pretreated WO_3/SiO_2. W^{5+} did not exist in WS–air and WS–N_2, while W^{5+} was observed in the catalysts pretreated by H_2 or H_2/N_2. When the H_2/N_2 ratio was increased from 1/9 to 1/1, the molar percentage of W^{5+} increased from 7.1% to 11.3%. For WS–H_2, the molar percentage of W^{5+} approached

Table 2
Binding energies and molar percentages of W^{5+} and W^{6+} species in WO_3/SiO_2 catalysts pretreated by different gases.

Catalysts	Binding energies for W_{4f} (eV)				W^{5+} (%)	W^{6+} (%)
	W^{6+} $4f_{5/2}$	W^{6+} $4f_{7/2}$	W^{5+} $4f_{5/2}$	W^{5+} $4f_{7/2}$		
WS–Air	38.0	35.9	N/A	N/A	0.0	100.0
WS–N_2	38.1	36.0	N/A	N/A	0.0	100.0
WS–1/9H_2/N_2	38.2	36.1	36.7	34.6	7.1	92.9
WS–1/1H_2/N_2	38.2	36.1	37.2	35.1	11.3	88.7
WS–H_2	38.2	36.1	36.9	34.8	17.7	82.3

17.7%. The relationship between the content of W^{5+} and the pretreatment gas was first reported here.

The WO_3/SiO_2 catalysts pretreated by different gases were studied by Raman spectroscopy. Raman peaks at 806, 710, and 268 cm^{-1} in Fig. 3, were assigned to the symmetric stretching mode of W–O, the bending mode of W–O, and the deformation mode of W–O–W in crystalline WO_3, respectively [40,41]. Moreover, a band around 979 cm^{-1} was assigned to the O=W=O bond of the isolated surface tetrahedral tungsten oxide [42–44]. In this work, WS–air in Fig. 3a and WS–N_2 in Fig. 3b exhibited characteristic Raman bands at 806, 710, and 268 cm^{-1}, corresponding to crystalline WO_3. For WS–1/9H_2/N_2 (Fig. 3c) and WS–1/1H_2/N_2 (Fig. 3d), the Raman peaks at 806 cm^{-1} became broader, and the peaks at 710 and 268 cm^{-1} disappeared, suggesting a gradual degradation of WO_3 crystallinity [45]. For WS–H_2 in Fig. 3e, all the Raman peaks of crystalline WO_3 almost disappeared, which is consistent with the reported Raman spectra of $WO_{2.9}$ [46]. The band at 979 cm^{-1} indicated the presence of isolated surface tetrahedral tungsten oxide in WS–air, WS–N_2, WS–1/9H_2/N_2, and WS–1/1H_2/N_2.

UV–vis DRS spectra of WO_3/SiO_2 pretreated by different gases are shown in Fig. 4. All catalysts showed two absorption bands at 215 and 250 nm, assigned to isolated $[WO_4]^{2-}$tetrahedral species and octahedral polytungstate species, respectively [47–49]. Huang et al. and Zhao et al. ascribed the absorption between 400 and 800 nm to reduced W species such as W^{4+} and W^{5+} [28,31]. In our present work, the absence of absorption between 450 and 800 nm in Fig. 4a and 4b indicated that W species in WS–air and WS–N_2 were in the W^{6+}state, which is consistent with the XRD and XPS results. For the H_2/N_2 or H_2-pretreated catalysts, the intensity of the band between 450 and 800 nm increased with the increase in H_2 content, suggesting the increase of the content of partially reduced W species, which is consistent with the XPS results. The formation of partially reduced W species by H_2 reduction of WO_3/SiO_2 allows the intervalence charge transfer from W^{5+} to W^{6+} in the substoichiometric WO_{3-x} [50], which explains the observation that the color of the catalyst gradually changed from yellow (WO_3) to deep blue ($WO_{2.92}$).

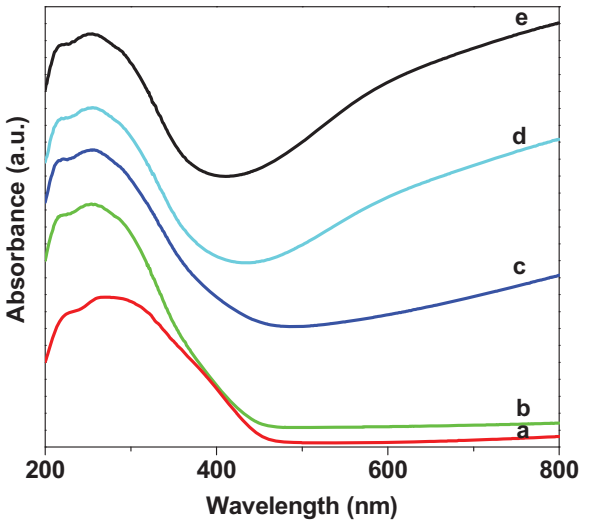

Fig. 4. (Color online.) UV–vis spectra of 6.0 wt% WO_3/SiO_2 catalysts pretreated with different gases: (a) WS–air; (b) WS–N_2; (c) WS–1/9H_2/N_2; (d) WS–1/1H_2/N_2; (e) WS–H_2.

H_2-TPR was used to monitor the reduction process of WS–air, WS–N_2, and WS–1/1H_2/N_2. As shown in Fig. 5a, the main H_2 consumption peak for WS–air was observed at 602–711 °C, with a very slight hump of H_2 consumption centered at 450 °C, while the first obvious H_2 consumption peak for WS–N_2 in Fig. 5b was at 417–520 °C, suggesting that WS–N_2 was more easily partially reduced by H_2 than WS–air. For WS–1/1H_2/N_2 in Fig. 5c, the first H_2 consumption peak was further shifted to lower temperatures starting at ca. 400 °C, indicating the easiest reducibility of WS–1/1H_2/N_2.

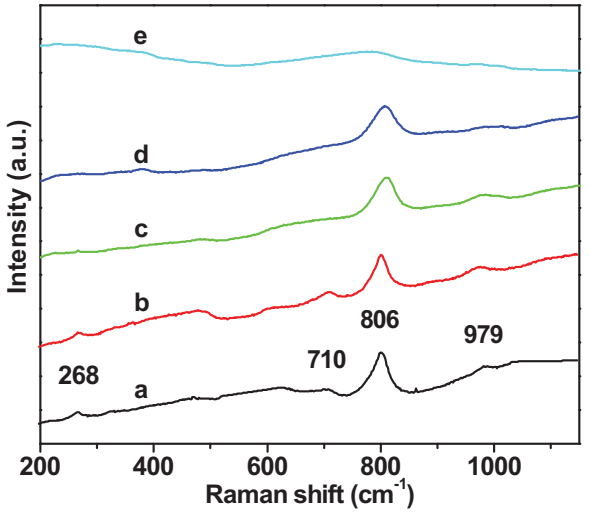

Fig. 3. (Color online.) Raman spectra of 6.0 wt% WO_3/SiO_2 pretreated with different gases: (a) WS–air; (b) WS–N_2; (c) WS–1/9H_2/N_2; (d) WS–1/1H_2/N_2; (e) WS–H_2.

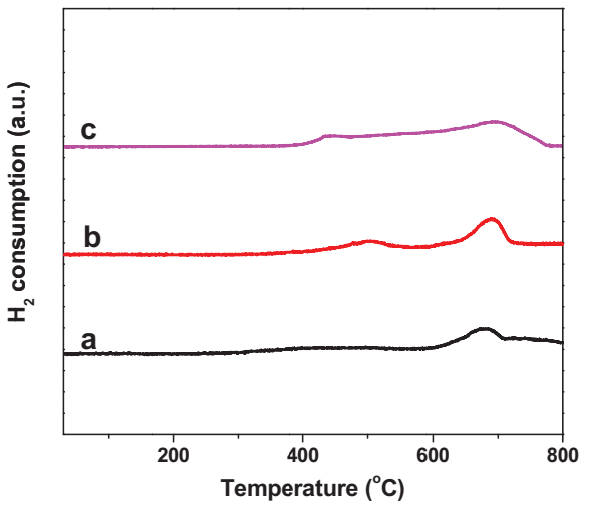

Fig. 5. (Color online.) H_2–TPR profiles of the pretreated 6.0 wt% WO_3/SiO_2 catalysts: (a) WS–air; (b) WS–N_2; (c) WS–1/1 H_2/N_2.

In the literature, the deep reduction of WO_3/SiO_2 catalysts was reported to be unfavorable to butene and ethene metathesis [28,51]. From the H_2-TPR data (Fig. 5), we can see that the deep reduction of catalysts occurred above 600 °C. That is the reason why we pretreated the catalysts (in air, N_2, $1/1H_2/N_2$, $1/9H_2/N_2$, or H_2) consistently at 400 °C. XPS data in Table 2 also confirmed that W^{6+} can be partially reduced to W^{5+} at 400 °C by H_2/N_2 or H_2, and the ratio of W^{5+}/W^{6+} can be adjusted by the ratio of H_2/N_2, thus providing opportunities for studying the effect of these parameters on catalytic performance.

TEM images of WS–N_2 and WS–$1/1H_2/N_2$ are shown in Fig. 6a and 6b, respectively. WO_3 particles were clearly observed on SiO_2. The HRTEM images of WS–N_2 and WS–$1/1H_2/N_2$ are shown in Fig. 6e and 6f, respectively. The lattice spacing (0.363 nm) of WS–N_2 in Fig. 6e is consistent with that of (200) planes of monoclinic WO_3 detected by XRD in Fig. 1c. Moreover, the lattice spacing with 0.392 nm of WS–$1/1H_2/N_2$ in Fig. 6f is consistent with that of (001) planes of tetragonal WO_3 detected by XRD in Fig. 1e.

The catalytic performance of WO_3/SiO_2 catalysts with different gas pretreatments was tested for metathesis of 1-butene and ethene in a fixed-bed reactor. The catalysts first converted 1-butene to 2-butene, and further catalyzed the metathesis of 2-butene and ethene to propene. In industrial processes, the reactant butene contains 1-butene and 2-butene, and MgO is used to convert the 1-butene fraction to 2-butene in order to obtain high product yield. In this study, WO_3/SiO_2 catalysts blended with MgO tablets were used for reaction testing. Below, the real catalyst systems were the WO_3/SiO_2 catalysts with MgO, unless otherwise specified.

To begin with, MgO was tested in the reaction to investigate the role of MgO. As shown in Fig. 7a, 34.2% conversion of 1-butene was achieved on MgO, and no propene was detected, suggesting that the only role of MgO was to convert 1-butene to 2-butene.

WS–$1/1H_2/N_2$ (without MgO) showed an average conversion of about 60% and an average propene selectivity of 74% during 5 h on stream (Fig. 7b). WS–$1/1H_2/N_2$ blended with MgO exhibited an average conversion of ca. 80% and an average propene selectivity of 89% (Fig. 7c). The enhancement in 1-butene conversion for the MgO-blended WO_3/SiO_2 is due to the extra 1-butene conversion provided by MgO. The increase in propene selectivity with the addition of MgO is due to the fact that MgO decreases the concentration of 1-butene, thus minimizing the formation of the high-molecular-weight compound via 1-butene oligomerization [52].

The catalytic performances of WO_3/SiO_2 with different gas pretreatments are summarized in Table 3, in which the product was sampled for online analysis at 2 h on stream. WS–air showed 33.5% of 1-butene conversion and 0.0% of propene selectivity, nearly the same as that of MgO, suggesting that WS–air was inactive. In contrast, WS–N_2 showed a conversion of 75.0% and a propene selectivity of 84.1%. All the H_2- and H_2/N_2-pretreated catalysts exhibited enhanced 1-butene conversion and propene selectivity. Among them, WS–$1/1H_2/N_2$ exhibited the highest 1-butene conversion and propene selectivity.

The propene yield (conversion × selectivity) of WO_3/SiO_2 catalysts decreased in the following order: WS–$1/1H_2/N_2$ (79.7%) > WS–H_2 (75.5%) > WS–$1/9H_2/N_2$ (66.8%) > WS–N_2 (63.1%) > WS–air (0.0%). Although WS–N_2 and WS–air exhibited similar XRD, XPS, Raman, and UV–vis data, WS–N_2 exhibited excellent 1-butene conversion and propene selectivity, whereas WS–air was inactive, indicating the formation of some active WO_3 phase and W species during metathesis on WS–N_2.

Postmortem analysis of the used WS–air, WS–N_2, and WS–$1/1H_2/N_2$ was carried out to investigate the change in

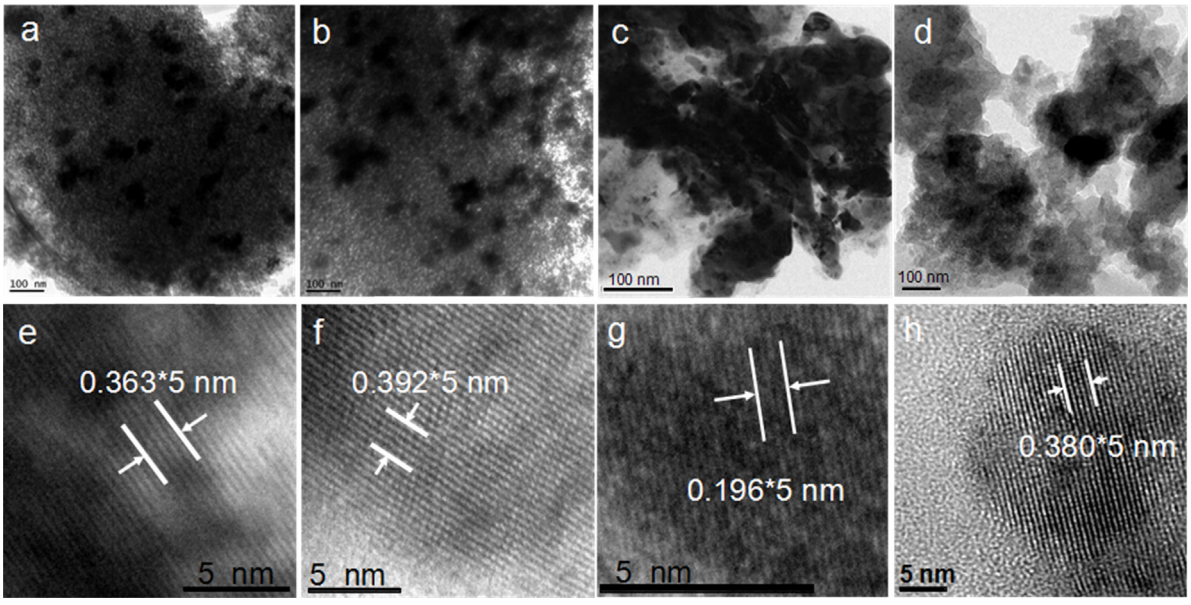

Fig. 6. TEM (top) and HRTEM (bottom) images of WS–N_2 (a, e); WS–$1/1H_2/N_2$ (b, f); the used WS–N_2 (c, g); the used WS–$1/1H_2/N_2$ (d, h). Scale bars of (a), (b), (c), and (d) are 100 nm; scale bars of (e), (f), (g), and (h) are 5 nm.

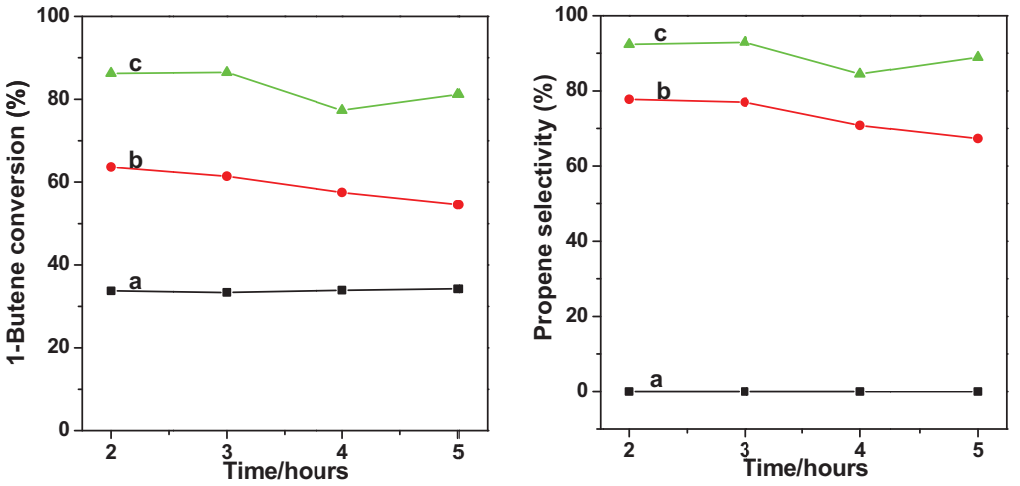

Fig. 7. (Color online.) 1-Butene conversion (left panel) and propene selectivity (right panel) over different catalysts: (a) MgO; (b) WS–1/1H_2/N_2; (c) WS–1/1H_2/N_2 + MgO. Reaction conditions: temperature: 280 °C; pressure: 3.0 MPa; C_2H_4 = 0.83 L/min and 1-C_4H_8 = 0.52 L/min; WO_3/SiO_2: 19.0 g; MgO: 76.0 g.

the physicochemical properties of the catalysts during the reaction. XRD patterns of the used catalysts are shown in Fig. 8. As shown in Fig. 8a, the used WS–air exhibited the same monoclinic WO_3 phase as WS–air before the reaction. In contrast, the WO_3 phase of WS–N_2 was gradually transformed from the monoclinic phase before the reaction (Fig. 1c) to the tetragonal phase after the reaction (Fig. 8b, 8c and 8d), suggesting the phase change during the reaction. Moreover, the WO_3 phase of WS–1/1H_2/N_2 transformed from the tetragonal phase before the reaction (Fig. 1e) to the $WO_{2.92}$ phase after the reaction (Fig. 8e), suggesting that the reactants or products could reduce the WO_3 phase under certain conditions. From the XRD data, it is inferred that the tetragonal WO_3 or partially reduced WO_{3-x} phase were active phases. Furthermore, air-pretreated monoclinic WO_3 phase was stable and inactive, whereas the N_2-pretreated monoclinic WO_3 phase could be transformed into an active tetragonal WO_3 phase during the reaction.

The phase change of WS–N_2 and WS–1/1H_2/N_2 after the reaction was further confirmed by TEM studies. TEM images of the used WS–N_2 and WS–1/1H_2/N_2 are shown in Fig. 6c and 6d, respectively, and HRTEM images of the used WS–N_2 and WS–1/1H_2/N_2 are shown in Fig. 6 g and 6 h, respectively. The lattice spacing with 0.196 nm in Fig. 6 g was consistent with that of (002) planes of the tetragonal WO_3, confirming the phase change from monoclinic WO_3 before the reaction to tetragonal WO_3 phase after the reaction for WS–N_2. Moreover, for the used WS–1/1H_2/N_2, the lattice spacing of 0.380 nm in Fig. 6 h was ascribed to that of (011) planes of $WO_{2.92}$, which is consistent with the phase change evidenced by the XRD pattern in Fig. 8e.

To investigate the oxidation state change of W species after the reaction, XPS studies of the used WS–air, WS–N_2, and WS–1/1 H_2/N_2 were conducted. As shown in Fig. 9a and Table 4, the used WS–air exhibited similar XPS data with WS–air before the reaction, showing the absence of reduced W^{5+}. However, XPS data of the used WS–N_2 collected at 20 min (Fig. 9b), 6 h (Fig. 9c), and 10 h (Fig. 9d) on stream illustrated the presence of a small portion of

Table 3
Catalytic performances of MgO and WO_3/SiO_2 catalysts with different gas pretreatments for metathesis of 1-butene and ethene to propene.

Catalysts[a]	1-Butene conversion (%)	Selectivity (%)	
		Propene	2-Butene
MgO	34.2	0.0	100.0
WS–air + MgO	33.5	0.0	100.0
WS–N_2 + MgO	75.0	84.1	15.9
WS–1/9H_2/N_2 + MgO	77.8	85.8	14.2
WS–1/1H_2/N_2 + MgO	86.3	92.3	7.7
WS–H_2 + MgO	83.4	90.5	9.5

[a] Reaction conditions: temperature: 280 °C; WHSV (1-butene + ethene) of 1.49 h^{-1}; pressure: 3.0 MPa; C_2H_4 = 0.83 L/min and 1-C_4H_8 = 0.52 L/min; WO_3/SiO_2: 19.0 g and MgO: 76.0 g; reaction time: 2 h.

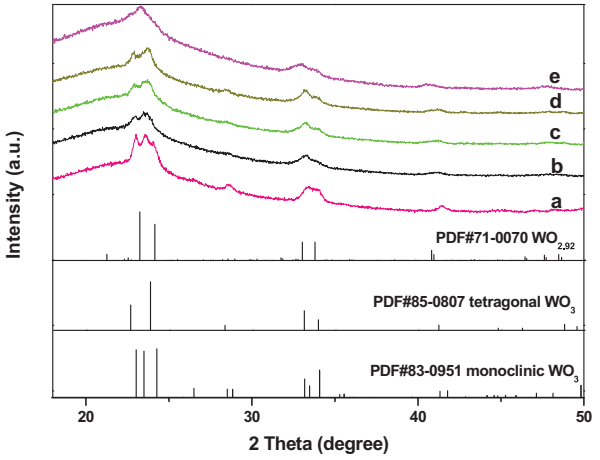

Fig. 8. (Color online.) XRD patterns of 6.0 wt% WO_3/SiO_2 catalysts pretreated with different gases and collected after reaction testing: (a) the used WS–air, 10 h (after a 10-h reaction); (b) the used WS–N_2, 20 min; (c) the used WS–N_2, 6 h; (d) the used WS–N_2, 10 h; (e) the used WS–1/1H_2/N_2, 10 h.

Table 4
Binding energies and molar percentages of W^{5+} and W^{6+} species in the used WO_3/SiO_2 catalysts pretreated by different gases.

Catalysts	Binding energies for W_{4f} (eV)				W^{5+} (%)	W^{6+} (%)
	W^{6+} $4f_{5/2}$	W^{6+} $4f_{7/2}$	W^{5+} $4f_{5/2}$	W^{5+} $4f_{7/2}$		
WS–Air–10 h	37.9	35.8	N/A	N/A	0.0	100.0
WS–N_2–20 min	38.0	35.9	36.7	34.6	5.0	95.0
WS–N_2–6 h	37.8	35.7	37.1	35.0	7.9	92.1
WS–N_2–10 h	37.9	35.8	36.8	34.7	14.3	85.7
WS–1/1H_2/N_2–10 h	38.2	36.1	37.1	35.0	17.8	82.2

W^{5+}, and the molar percentage of W^{5+} increased from 5.0% at 20 min to 14.3% at 10 h, indicating the formation of some W^{5+} during the reaction. The appearance of W^{5+} for WS–N_2 during the reaction is consistent with the H_2-TPR data in Fig. 5, where WS–N_2 was easier to be reduced than WS–air. Moreover, the molar percentage of W^{5+} of the used WS–1/1H_2/N_2 increased from 11.3% before the reaction in Table 2 to 17.8% after the reaction, as can be seen in Table 4, further confirming that the reactants or products in the metathesis of 1-butene and ethene can partially reduce WO_3.

The W^{5+} content of WS–N_2 was significantly increased from 0.0% to 14.3% during the 10-h reaction, while the W^{5+} content of WS–1/1H_2/N_2 was slowly increased from 11.3% to 17.8% during 10 h on stream. The significant increase in W^{5+} for WS–N_2 may significantly influence the catalytic performance of WS–N_2 during the first several hours on stream if the W^{5+} species were catalytically active. The catalytic studies mentioned above were carried out at 3.0 MPa and 280 °C in a 200-mL fixed-bed reactor with the 3–5-mm catalysts lumps. Under the above reaction conditions, 1-butene liquid at 3.0 MPa had to be pumped into a preheater to gasify. Because 1-butene contacted the catalyst layer later than ethene, the early stage of reaction cannot be correctly sampled and analyzed. To correctly investigate the initial stage of reaction, the reaction was carried out at 0.1 MPa and 430 °C in a 5-mL fixed-bed reactor with the 20–40 mesh catalysts. The 1-butene and

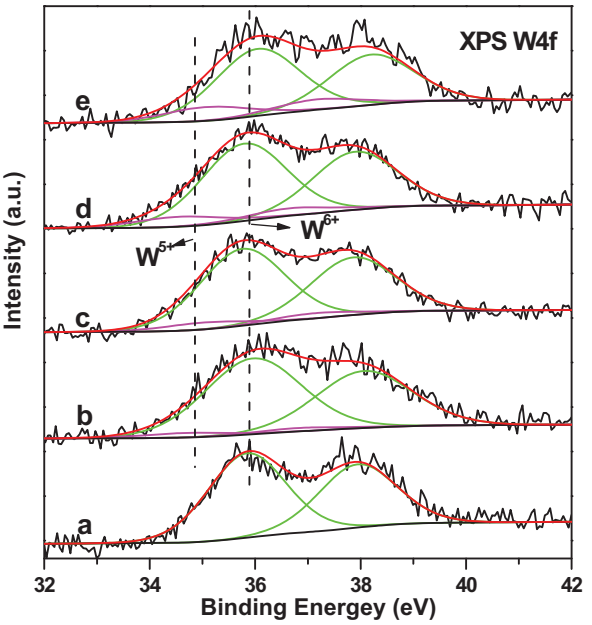

Fig. 9. (Color online.) XPS spectra of 6.0 wt% the used WO_3/SiO_2 catalysts pretreated with different gases and collected after reaction testing. (a) WS–air, 10 h (after a 10-h reaction); (b) WS–N_2, 20 min; (c) WS–N_2, 6 h; (d) WS–N_2, 10 h; (e) WS–1/1H_2/N_2, 10 h.

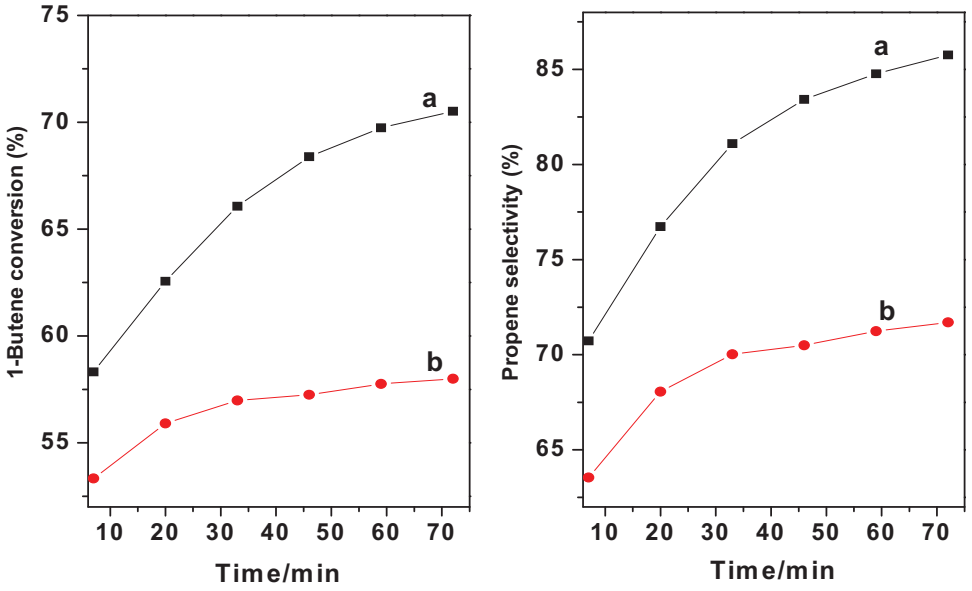

Fig. 10. (Color online.) 1-butene conversion (left panel) and propene selectivity (right panel) over different catalysts: (a) 1 g WS–N_2 + 1.5 g MgO; (b) 1 g WS–1/1H_2/N_2 + 1.5 g MgO. T = 430 °C; P = 0.1 MPa; ethene, 10 mL/min; 1-butene, 5 mL/min.

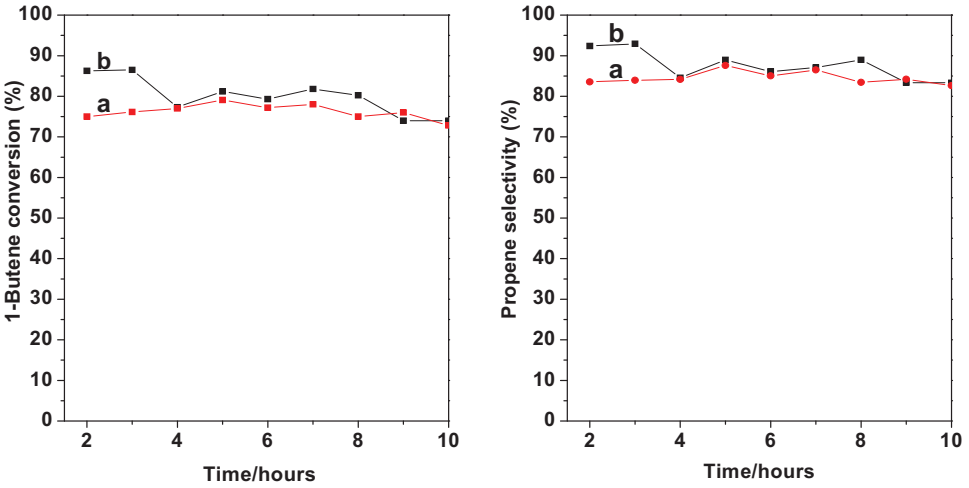

Fig. 11. (Color online.) The reaction profiles of 1-butene conversion (left panel) and propene selectivity (right panel) of gas-pretreated catalysts: (a) WS–N_2 + MgO; (b) WS–$1/1H_2/N_2$ + MgO. Reaction conditions: temperature, 280 °C; WHSV-(1-butene + ethene), 1.49 h^{-1}; C_2H_4 = 0.83 L/min and 1-C_4H_8 = 0.52 L/min; pressure, 3.0 MPa; WO_3/SiO_2, 19.0 g, and MgO, 76.0 g.

ethene at 0.1 MPa were fed into the reactor in a gas state so that the early stage of the reaction can be studied.

The initial catalytic performances at 0.1 MPa of WS–N_2 and WS–$1/1H_2/N_2$ in a microreactor are shown in Fig. 10. The reaction was carried out at 430 °C to clearly observe the catalytic performance change with the reaction time. As shown in Fig. 10b, 1-butene conversion and propene selectivity over WS–$1/1H_2/N_2$ increased slowly during the first 80 min. However, WS–N_2 exhibited a significant growth of catalytic activity and selectivity (Fig. 10a). The phase change from monoclinic to tetragonal by postmortem XRD study and the appearance of W^{5+} during the reaction by postmortem XPS study can explain the significant activity growth during the early stage of reaction for WS–N_2, and the tetragonal WO_3 phase and W^{5+} were ascribed to the active phase and species. The appearance of W^{5+} was necessary for the formation of sufficiently active and stable W carbene species responsible for metathesis [53,54]. Under these reaction conditions, WS–N_2 illustrated a better catalytic performance than WS–$1/1H_2/N_2$, suggesting that WS–N_2 was more suitable for high-temperature metathesis at 0.1 MPa.

The reaction profiles of 1-butene conversion and propene selectivity over WS–N_2 and WS–$1/1H_2/N_2$ are shown in Fig. 11. The reaction was again carried out at 3.0 MPa and 280 °C in a 200-mL fixed-bed reactor with the 3–5-mm catalysts lumps. The 1-butene conversion/propene selectivity of WS–$1/1H_2/N_2$ decreased from 86.3%/92.3%

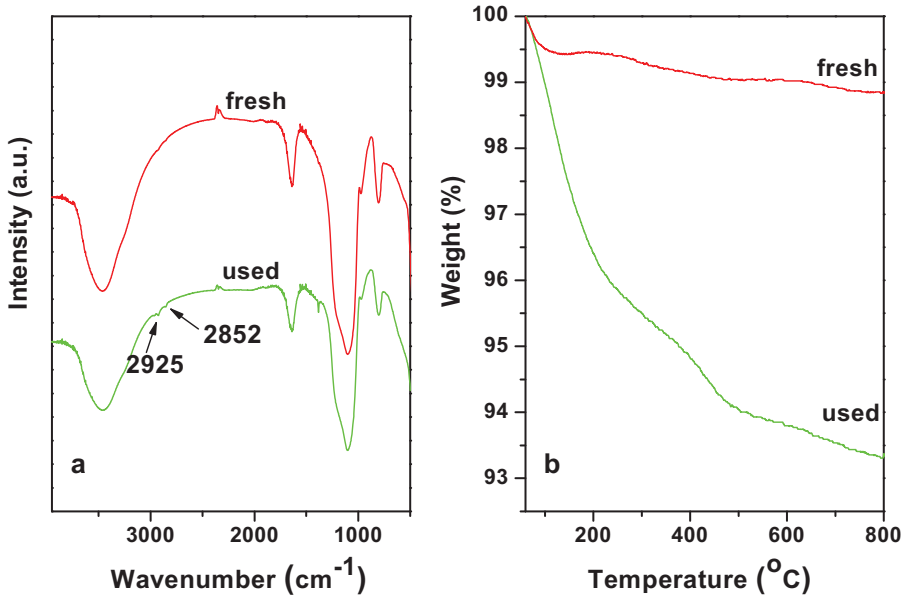

Fig. 12. (Color online.) (a) FT-IR spectra of the fresh and used WS–$1/1H_2/N_2$; (b) TGA profiles of the fresh and used WS–$1/1H_2/N_2$.

to 74.0%/83.3% after 10 h on stream. For comparison, the 1-butene conversion/propene selectivity of WS–N_2 decreased from 75%/83.5% to 72.8%/82.7% after 10 h on stream.

It should be emphasized here that the reaction conditions in this study were more critical than those in industrial processes. Pure 1-butene was used in this work, while industrial processes used mixtures of 1-butene and 2-butene, and 2-butene was more favorable to the metathesis of butene and ethene to propene [55–58].

In the literature, the deep reduction of WO_x was found to be unfavorable to metathesis [28,51]. In this study, the XRD patterns of the used WS–1/1H_2/N_2 revealed the formation of a $WO_{2.92}$ phase after the reaction. Therefore, no deep reduction occurred.

FT-IR spectra and TGA profiles of the fresh and used WS–1/1H_2/N_2 are illustrated in Fig. 12. Some organic residues on the catalyst were indicated by the appearance of the antisymmetric stretching vibration of the methyl group at 2925 cm^{-1} in FT-IR spectra of the used catalyst in Fig. 12a [59]. Moreover, TGA analysis in Fig. 12b provides another evidence of organic residues on the used catalyst. Compared with the fresh catalyst, an additional 5.5 wt% of weight loss of the used catalyst was observed. The catalyst's deactivation is possibly due to the deposition of heavy organic compounds onto catalysts during the reaction.

4. Conclusions

WO_3/SiO_2 catalysts pretreated by air, N_2, 1/9H_2/N_2, 1/1H_2/N_2 and pure H_2 were characterized by XRD, N_2 adsorption–desorption, Raman, UV–vis, TGA, FT-IR, TEM, XPS and H_2-TPR, and tested in the metathesis of 1-butene and ethene to propene. WS–air with monoclinic WO_3 phase was inactive, and the monoclinic WO_3 phase cannot be transformed into an active phase during the reaction. WS–N_2, WS–H_2/N_2, and WS–H_2 showed enhanced catalytic performance. The tetragonal WO_3 and partially reduced $WO_{2.92}$ were active phases for the reaction. The tetragonal WO_3 phase can be formed by pretreatment in H_2/N_2 mixtures or from the transformation of monoclinic WO_3 of WS–N_2 during the reaction. All active WO_3/SiO_2 catalysts after the reaction contained W^{5+} species, which are assigned to active W species.

It should be cautioned that the conclusion about the active W species and crystallographic phases may be dependent on the SiO_2 nature of the support, which may not be the case with other supported catalysts. In addition, the characterization in our study was conducted ex situ, but not in situ. The interaction between the reactants/intermediates and the active sites may be dynamic during the reaction. Additional work is still needed to better understand the reaction mechanism.

As for the implication of the current work to industrial catalysis, we would like to propose that perhaps the pretreatment conditions (i.e., pretreatment gas, temperature, duration of pretreatment) should be strictly controlled to get the best performance in olefin metathesis. In addition, the option of using in situ activation of catalysts (i.e., for WS–N_2 during the reaction) should be avoided, just in order to get stable activity and selectivity in industrial reactors.

Acknowledgements

The authors are grateful for the financial support from the Ministry of Science and Technology of China under Grant 2012DFA40550, and Ningbo Municipal Natural Science Foundation under Grant 2013A610038.

References

[1] R.L. Banks, G.C. Bailey, Ind. Eng. Chem. Prod. Res. Dev. 3 (1964) 170–173.
[2] R.R. Schrock, Angew. Chem. Int. Ed. 45 (2006) 3748–3759.
[3] R.H. Grubbs, Angew. Chem. Int. Ed. 45 (2006) 3760–3765.
[4] Y. Chauvin, Angew. Chem. Int. Ed. 45 (2006) 3740–3747.
[5] K.J. Ivin, J.C. Mol, Olefin metathesis and metathesis polymerization, 2nd ed., Academic Press, London, 1997.
[6] J.C. Mol, J. Mol. Catal. A: Chem. 213 (2004) 39–45.
[7] R.H. Grubbs, T.K. Brunck, J. Am. Chem. Soc. 94 (1972) 2538–2540.
[8] V.M. Benitez, C.A. Querini, N.S. Figoli, Appl. Catal. A 252 (2003) 427–436.
[9] D. Lokhat, M. Starzak, M. Stelmachowski, Appl. Catal. A 351 (2008) 137–147.
[10] D.P. Debecker, B. Schimmoeller, M. Stoyanova, C. Poleunis, P. Bertrand, U. Rodemerck, E.M. Gaigneaux, J. Catal. 277 (2011) 154–163.
[11] X.J. Li, W.P. Zhang, S.L. Liu, L.Y. Xu, X.W. Han, X.H. Bao, J. Phys. Chem. C 112 (2008) 5955–5960.
[12] X. Teng, D.R. Cefalo, R.R. Schrock, A.H. Hoveyda, J. Am. Chem. Soc. 124 (2002) 10779–10784.
[13] L.G. Duquette, R.C. Cieslinsky, C.W. Jung, P.E. Garrou, J. Catal. 90 (1984) 362–365.
[14] B. Mitra, X. Gao, I.E. Wachs, A.M. Hirt, G. Deo, Phys. Chem. Chem. Phys. 3 (2001) 1144–1152.
[15] J.C. Mol, Catal. Today 51 (1999) 288–289.
[16] R. Spronk, J.A.R. Vanveen, J.C. Mol, J. Catal. 144 (1993) 472–483.
[17] R.L. Banks, Appl. Ind. Catal. 4 (1984) 215.
[18] A. Rodriguez-Ramos, Guerrero-Ruiz, N. Horns, P.P. Ramirezdela, J.L.G. Fierro, J. Mol. Catal. A: Chem. 95 (1995) 147–154.
[19] W. Michael McCaulley, US 5300718 1994.
[20] R.C. Luckner, G.B. Wills, J. Catal. 28 (1973) 83–91.
[21] S.K. Gangwal, J. Fathi-kalajahi, G.B. Wills, Ind. Eng. Chem. Prod. Res. Dev. 16 (1977) 193–268.
[22] F. Pennella, R.L. Banks, J. Catal. 31 (1973) 304–308.
[23] A. Andreini, J.C. Mol, J. Colloid Interface Sci. 84 (1985) 57–65.
[24] R. Thomas, J.A. Moulijn, J. Mol. Catal. 8 (1980) 161–174.
[25] S.J. Choung, S.W. Weller, Ind. Eng. Chem. Prod. Res. Dev. 22 (1983) 662–665.
[26] R. Westhoff, J.A. Moulijn, J. Catal. 46 (1977) 414–416.
[27] A.G. Basrur, S.R. Patwardhan, S.N. Was, J. Catal. 127 (1991) 86–95.
[28] S.J. Huang, S.L. Liu, W.J. Xin, J. Bai, S.J. Xie, Q.X. Wang, L.Y. Xu, J. Mol. Catal. 226 (2005) 61–68.
[29] M.I. Zaki, N.E. Fouad, S.A.A. Mansour, A.I. Muftah, Thermochim. Acta 523 (2011) 90–96.
[30] E. Lassner, W.-D. Schubert, Tungsten: properties, chemistry, technology of the element, alloys, and chemical compounds, Kluwer Academic/Plenum Publishers, New York, 1999.
[31] Q.F. Zhao, S.L. Chen, J.S. Gao, C.M. Xu, Transit. Metal Chem. 34 (2009) 621–627.
[32] S. Doniach, M. Sunjic, J. Phys. C: Solid State Phys. 3 (1970) 285–291.
[33] P. Biloen, G.T. Pott, J. Catal. 30 (1973) 169–174.
[34] X.L. Yang, W.L. Dai, R.H. Gao, K.N. Fan, J. Catal. 249 (2007) 278–288.
[35] M. Valigi, D. Gazzoli, I. Pettiti, G. Mattei, S. Colonna, S.D. Rossi, G. Ferraris, Appl. Catal. A 231 (2002) 159–172.
[36] P. Charton, L. Gengembre, P. Armand, J. Solid State Chem. 168 (2002) 175–183.
[37] A.P. Shpak, A.M. Korduban, M.M. Medvedskij, V.O. Kandyba, J. Electron. Spectrosc. Relat. Phenom. 156 (2007) 172–175.
[38] M.S. Bazarjani, M. Hojamberdiev, K. Morita, G.Q. Zhu, G. Cherkashinin, C. Fasel, T. Herrmann, H. Bretizke, A. Gurlo, R. Riede, J. Am. Chem. Soc. 135 (2013) 4467–4475.
[39] R.J. Colton, A.M. Guzman, J.W. Rabalais, Acc. Chem. Res. 11 (1978) 170–176.
[40] E.L. Lee, I.E. Wachs, J. Phys. Chem. C 112 (2008) 6487–6489.
[41] F. Figueras, J. Palomeque, S. Loridant, C. Fèche, N. Essayem, G. Gelbard, J. Catal. 226 (2004) 25–31.

[42] L. Salavati Jr., L.E. Makovsky, J.M. Stencel, F.R. Brown, D.M. Hercules, J. Phys. Chem. 85 (1981) 3700–3707.
[43] E.I. Ross-Medgaarden, W.V. Knowles, T. Kim, M.S. Wong, W. Zhou, C.J. Kiely, I.E. Wachs, J. Catal. 256 (2008) 108–125.
[44] J.A. Horsely, I.E. Wachs, J.M. Brown, G.H. Via, F.D. Hardcastle, J. Phys. Chem. 91 (1987) 4014–4020.
[45] G.M. Wang, Y.C. Ling, H.Y. Wang, X.Y. Yang, C.C. Wang, J.Z. Zhang, Y. Li, Energy Environ. Sci. 5 (2012) 6180–6187.
[46] J.G. Liu, Y. Zhao, Z.J. Zhang, J. Phys.: Condens. Matter 15 (2003) L453.
[47] A. Ramanathan, B. Subramaniam, D. Badloe, U. Hanefeld, R.M. Maheswari, J. Porous Mater. 19 (2012) 961–968.
[48] X.L. Yang, R.H. Gao, W.L. Dai, K.N. Fan, J. Phys. Chem. C 112 (2008) 3819–3826.
[49] J. Ramirez, A.G. Alejandre, J. Catal. 170 (1997) 108–122.
[50] H.L. Wang, T. Lindgren, J.J. He, A. Hagfeldt, S.E. Lindquist, J. Phys. Chem. B 104 (2000) 5686–5696.
[51] A. Spamer, T.I. Dube, D.J. Moodley, C.V. Van, J.M. Botha, Appl. Catal. A 255 (2003) 133–142.
[52] B. Hu, H. Liu, K. Tao, C.R. Xiong, S.H. Zhou, J. Phys. Chem. 117 (2013) 26385–26395.
[53] B. Zhang, N. Liu, Q.S. Lin, D. Jin, J. Mol. Catal. 65 (1991) 15–28.
[54] B.N. Shelimov, L.V. Elev, V.B. Kazansky, J. Catal. 98 (1986) 70–81.
[55] D.R. Hua, S.L. Chen, G.M. Yuan, Y.L. Wang, L. Zhang, Transit. Metal Chem. 36 (2011) 245–248.
[56] K. Weiss, G. Lössel, Angew. Chem. Int. Ed. 28 (1989) 62–64.
[57] M. Taoufik, E.L. Roux, J. Thivolle-Cazat, J.M. Basset, Angew. Chem. Int. Ed. 46 (2007) 7202–7205.
[58] E. Mazoyer, K.C. Szeto, S. Norsic, A. Garron, J.M. Basset, C.P. Nicholas, M. Taoufik, ACS Catal. 1 (2011) 1643–1646.
[59] T. Noguchi, M. Sugiura, Biochem. 42 (2003) 6035–6042.